

## Wavelength selection by dielectric-loaded plasmonic components

Tobias Holmgaard,<sup>1,a)</sup> Zhuo Chen,<sup>1</sup> Sergey I. Bozhevolnyi,<sup>2</sup> Laurent Markey,<sup>3</sup> Alain Dereux,<sup>3</sup> Alexey V. Krasavin,<sup>4</sup> and Anatoly V. Zayats<sup>4</sup>

<sup>1</sup>Department of Physics and Nanotechnology, Aalborg University, Skjernvej 4A, DK-9220 Aalborg Øst, Denmark

<sup>2</sup>Institute of Sensors, Signals and Electrotechnics (SENSE), University of Southern Denmark, Niels Bohrs Allé 1, DK-5230 Odense M, Denmark

<sup>3</sup>Institut Carnot de Bourgogne, UMR 5209 CNRS-Université de Bourgogne, 9 Av. A. Savary, BP 47 870, F-21078 Dijon Cedex, France

<sup>4</sup>Centre for Nanostructured Media, IRCEP, The Queen's University of Belfast, Belfast BT7 1NN, United Kingdom

(Received 31 October 2008; accepted 6 January 2009; published online 6 February 2009)

Fabrication, characterization, and modeling of waveguide-ring resonators and in-line Bragg gratings for wavelength selection in the telecommunication range are reported utilizing dielectric-loaded surface plasmon-polariton waveguides. The devices were fabricated by depositing subwavelength-sized polymer ridges on a smooth gold film using industrially compatible large-scale UV photolithography. We demonstrate efficient and compact wavelength-selective filters, including waveguide-ring resonators with an insertion loss of  $\sim 2$  dB and a footprint of only  $150 \mu\text{m}^2$  featuring narrow bandwidth ( $\sim 20$  nm) and high contrast ( $\sim 13$  dB) features in the transmission spectrum. The performance of the components is found in good agreement with the results obtained by full vectorial three-dimensional finite element simulations. © 2009 American Institute of Physics. [DOI: 10.1063/1.3078235]

Surface plasmon polaritons (SPPs), being light waves coupled to free electron oscillations in metals,<sup>1,2</sup> can be laterally confined below the diffraction limit using subwavelength metal structures.<sup>2-7</sup> Plasmonic components open an enticing perspective of combining high operational bandwidth of photonic components with subwavelength dimensions of SPP waveguides.<sup>6,7</sup> Recently developed dielectric-loaded SPP waveguides (DLSPWs), utilizing high effective indices of SPP modes guided by dielectric ridges on smooth metal films,<sup>8-13</sup> represent an attractive alternative to other plasmonic technologies by virtue of being naturally compatible with different dielectrics and industrial fabrication using UV lithography.<sup>14,15</sup> Preliminary investigations indicated that DLSPW-based components feature relatively low bend and propagation losses<sup>14,15</sup> but their potential for wavelength selection, a crucial functionality for any photonic circuit, has so far not been explored.

Here we report on the investigation of main wavelength-selective DLSPW components such as waveguide-ring resonators (WRRs) and in-line Bragg gratings (BGs) exploited for wavelength selection in the telecommunication range.

All devices were fabricated using deep-UV lithography (wavelength of  $\sim 250$  nm) with a Süss Microtech MJB4 mask aligner in the vacuum contact mode and a  $\sim 550$ -nm-thick layer of polymethyl-methacrylate (PMMA) resist spin coated on a 60-nm-thin gold film, which was supported by a thin glass substrate. Typically, the width of the produced waveguides, inspected with scanning electron microscopy (SEM), was close to 500 nm ensuring the single mode (and close to optimum) DLSPW operation.<sup>10</sup> The performance of the fabricated components was characterized using a collection scanning near-field optical microscope

(SNOM) having an uncoated fiber tip used as a probe and an arrangement for SPP excitation ( $\lambda = 1500$ – $1620$  nm) in the Kretschmann configuration,<sup>1</sup> as described in detail elsewhere.<sup>14,15</sup> All waveguide structures were connected to funnel structures [Fig. 1(a)], facilitating efficient excitation of the DLSPW mode,<sup>16</sup> with the further improvement in the DLSPW mode, was excited *directly* inside the taper by matching the excitation angle (under total internal reflection), resulting in SNOM images of high quality.<sup>16</sup>

The first wavelength-selective components to be studied were WRRs designed to have 5- $\mu\text{m}$ -radius rings separated by different gaps from straight DLSPWs [Fig. 1(a)]. Using the SNOM imaging it was found that while the WRRs with the gaps (the minimum distance between the edge of the waveguide and the edge of the ring [Fig. 1(b)]) designed, having the widths  $g \cong 2.53$  and  $1.53 \mu\text{m}$ , did not exhibit noticeable ring-DLSPW mode excitation, the WRR with the gap  $g \cong 0.53 \mu\text{m}$  [Fig. 1(b)] featured very efficient ring excitation and well-pronounced wavelength-dependent behavior [Figs. 1(d)–1(g)]. The SEM image of the  $g \cong 0.53 \mu\text{m}$  WRR reveals that the gap is not completely resolved as some residual PMMA resistance still exists in the gap [Fig. 1(b)], which is likely to cause slightly more coupling to the ring than expected for that gap size. Note that the WRR transmission [Fig. 1(h)] was evaluated using the input and output waveguide cross sections separated by  $10 \mu\text{m}$  [Fig. 1(c)], a propagation length that alone introduces  $\sim 20\%$  of loss as estimated from the DLSPW propagation length of  $\sim 50 \mu\text{m}$ .

In general, the WRR transmission is expected to be periodic with respect to the phase accumulated by the ring-DLSPW mode per circulation and can be described with the following expression:<sup>17</sup>

<sup>a)</sup>Electronic mail: holmgaard@nano.aau.dk.

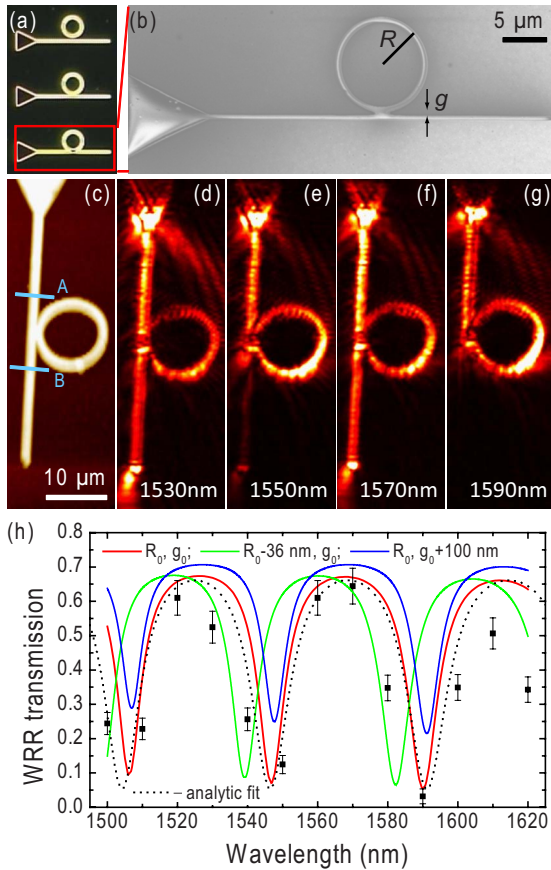


FIG. 1. (Color online) Plasmonic WRR. (a) Dark-field microscope image of fabricated WRRs with different gaps. (b) SEM image along with (c) topographical, and [(d)–(g)] near-field optical [ $\lambda=(d)$  1530, (e) 1550, (f) 1570, and (g) 1590 nm] SNOM images of the investigated WRR. (h) Transmission WRR spectra determined experimentally from SNOM images [similar to (d)–(g)] using an analytic fit by Eq. (1) and with 3D-FEM simulations for 10- $\mu\text{m}$ -long input-to-output propagation [marked by lines A and B in (c)] and for three sets of WRR parameters: ring radius  $R_0=5486$  nm and gap width  $g_0=250$  nm,  $R=5450$  nm and  $g=250$  nm,  $R=5486$  nm, and  $g=350$  nm.

$$T = \exp(-l/L_{SP}) \frac{\alpha^2 + t^2 - 2\alpha t \cos \theta}{1 + \alpha^2 t^2 - 2\alpha t \cos \theta}, \quad (1)$$

where  $\theta = (2\pi/\lambda)n_{\text{eff}}(\lambda)2\pi R$ . The first factor in Eq. (1) reflects the power loss incurred by the propagation over the distance  $l=10$   $\mu\text{m}$  related to the DLSPPW propagation length  $L_{SP} \sim 50$   $\mu\text{m}$ .  $\alpha$  is the mode propagation and bend loss in the ring,  $t$  is the mode transmission through the coupling region in the straight waveguide,<sup>17</sup>  $\lambda$  is the light wavelength in air,  $R$  is the ring radius, and  $n_{\text{eff}}(\lambda)$  is the DLSPPW effective index, whose dispersion has to be taken into account. When fitting the experimental data [Fig. 1(h)], we used the calculated<sup>10</sup> mode dispersion resulting in  $n_{\text{eff}}(\lambda) \cong 1.61 - 0.25\lambda(\mu\text{m})$ , finding other parameters to be at  $\alpha \cong 0.55$ ,  $t \cong 0.7$ , and  $R \cong 5.43$   $\mu\text{m}$ . Note that the fitted mode loss in the ring  $\alpha$  implies that the bend loss amounted to  $\sim 0.36$  dB/rad was indeed relatively small as expected. Finally, it is seen that the investigated WRR features nearly *complete extinction* (reaching  $\sim 13$  dB at 1590 nm) with a  $\sim 20$ -nm bandwidth, showing thereby much better performance than the channel plasmon polariton (CPP)-based WRRs of the same size.<sup>18</sup>

Full three-dimensional finite element (3D-FEM) simulations of the WRR transmission using the ring radius  $R$  and

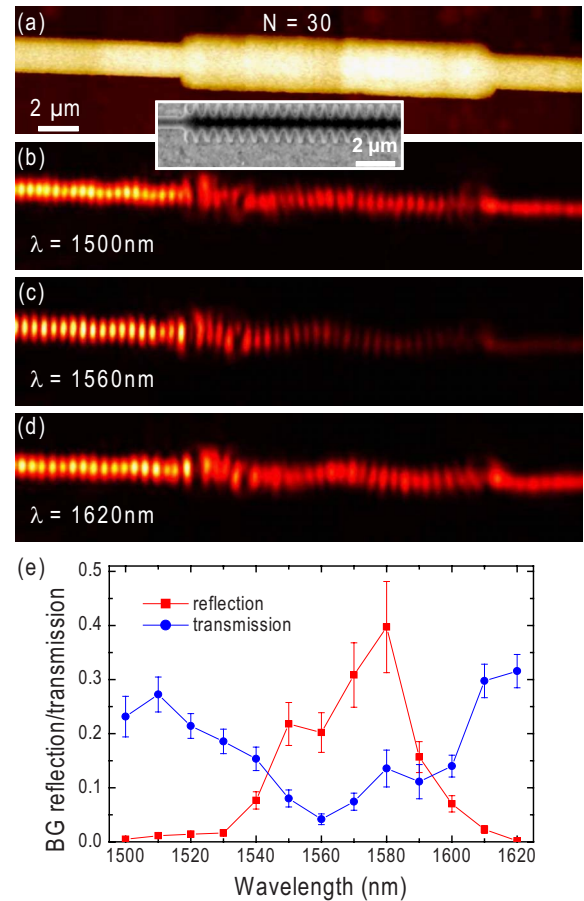


FIG. 2. (Color online) Plasmonic BG. (a) Topographical and [(b)–(d)] near-field optical [ $\lambda=(b)$  1500, (c) 1560, and (d) 1620 nm] SNOM images of an 18- $\mu\text{m}$ -long BG with the period of 600 nm along with an inset showing an SEM image of the BG section. (e) BG reflection and transmission spectra determined experimentally from SNOM images similar to (b)–(d).

ring-waveguide gap  $g$  as fitting parameters are presented in Fig. 1(h). It is seen that the WRR transmission calculated for  $R_0=5486$  nm and  $g_0=250$  nm, being close to the analytic fit, reproduces well the experimental features. More importantly, the simulations predict the observed trend of increasing the contrast with wavelength much better than the fit by virtue of taking consistently into account the DLSPPW dispersion influencing the phase delay, insertion loss, and coupling strength. Note that the positions of the minima are very sensitive to the ring radius, whereas their level is strongly influenced by the gap width (controlling the coupling strength), indicating the tolerance level in the WRR design and fabrication.

Wavelength selection can also be realized with diffraction gratings, e.g., by using in-line BG-based filters well known in integrated optics and introduced recently for long range SPP waveguides.<sup>19,20</sup> We made use of the dependence of DLSPPW mode index on the dielectric ridge width,<sup>10</sup> and fabricated 600-nm-period step-in-width (from 500 nm to 2  $\mu\text{m}$ ) BGs with 300-nm-long intervals between wide BG sections and containing different number of periods:  $N=10$ , 20, 30, and 50. The DLSPPW mode index variation was estimated<sup>10</sup> between  $\sim 1.2$  and 1.4 at  $\lambda \sim 1.55$   $\mu\text{m}$ , so that the BG transmission minimum was expected at  $\lambda \cong 2\Lambda n_{\text{av}} = 1.56$   $\mu\text{m}$  ( $\Lambda$  and  $n_{\text{av}}$  being the grating period and average DLSPPW mode index). The advantage of this design is that the BG fabrication does not require additional processing (as,

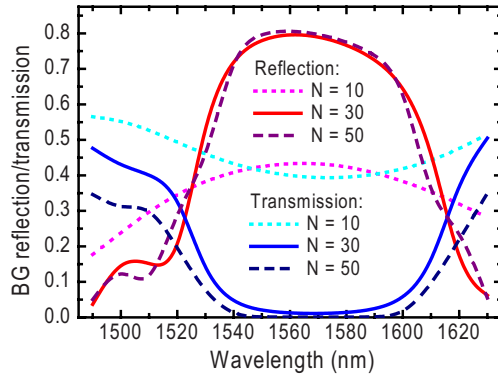


FIG. 3. (Color online) Reflection and transmission BG spectra calculated with 3D-FEM simulations for the 600 nm period BGs with different numbers of grating periods:  $N=10$ , 30, and 50.

for example, step-in-depth gratings<sup>20</sup>). However, UV lithography resolution is more critical here than in the above case of the WRRs because of small-sized ( $\sim 300$  nm) features throughout the whole BG length, resulting in more pronounced proximity effects, seen as a rounding of the gratings, affecting the geometry of fabricated BGs [see inset in Fig. 2(a)]. Still, the 30-period BG exhibited well-defined Bragg reflection and extinction in transmission with the wavelength interval of 1540–1600 nm (Fig. 2). Note that relatively low transmission levels ( $\sim 0.3$ ) observed outside of the band gap are partially accounted for by the DLSPW mode propagation loss reducing alone the transmission to  $\sim 0.7$ . In comparison, the 20-period BG performed similarly but with considerably weaker Bragg reflection ( $\sim 0.15$ ) and extinction ( $\sim 0.13$ ), while the 50-period BG featured about the same Bragg reflection but very low transmission ( $< 0.15$ ) at all wavelengths.

The 3D-FEM simulations of BG reflection and transmission (Fig. 3) showed all the main features observed: the well defined band gap (seen in both reflection and transmission) within the range of 1540–1600 nm, the similar reflection for  $N=30$  and  $N=50$  but lower transmission for the latter, and the rather weak band-gap effects for  $N=10$ . However, the simulated BG characteristics are much better with respect to the insertion loss (most probably due to weaker out-of-plane scattering), a circumstance that we attribute to the structural imperfections.

In conclusion, in using industrially compatible large-scale UV-lithography-based fabrication and exploiting the

principles of DLSPW-based plasmonic technology, we have realized efficient and compact wavelength-selective components: WRRs and BGs, operating at telecommunication wavelengths. In particular, we have demonstrated the WRR with an insertion loss of  $\sim 2$  dB and a footprint of only  $150 \mu\text{m}^2$  ( $\sim 60\lambda^2$ ) featuring deep minima (with the contrast of up to  $\sim 13$  dB) in its wavelength transmission spectrum with a bandwidth of  $\sim 20$  nm. Taking into account that this technology is naturally compatible with different dielectrics, one can envisage the development of ultracompact plasmonic components utilizing thermo-, electro-, magneto-, acousto-, and nonlinear optical effects as well as being integrated with electrical circuits.

This work was supported by EC FP6 STREP PLASMO-COM. A.V.Z. also acknowledge the financial support from EPSRC (UK).

<sup>1</sup>H. Raether, *Surface Plasmons on Smooth and Rough Surfaces and on Gratings*, 1st ed. (Springer, Berlin, 1988).

<sup>2</sup>W. L. Barnes, A. Dereux, and T. W. Ebbesen, *Nature (London)* **424**, 824 (2003).

<sup>3</sup>S. A. Maier and H. A. Atwater, *J. Appl. Phys.* **98**, 011101 (2005).

<sup>4</sup>S. Lal, S. Link, and N. J. Halas, *Nat. Photonics* **1**, 641 (2007).

<sup>5</sup>W. A. Murray and W. L. Barnes, *Adv. Mater.(Weinheim, Ger.)* **19**, 3771 (2007).

<sup>6</sup>R. Zia, J. A. Schuller, A. Chandran, and M. L. Brongersma, *Mater. Today* **9**, 20 (2006).

<sup>7</sup>T. W. Ebbesen, C. Genet, and S. I. Bozhevolnyi, *Phys. Today* **61**, 44 (2008).

<sup>8</sup>C. Reinhardt, S. Passinger, B. N. Chichkov, C. Marquart, I. P. Radko, and S. I. Bozhevolnyi, *Opt. Lett.* **31**, 1307 (2006).

<sup>9</sup>B. Steinberger, A. Hohenau, H. Ditlbacher, A. L. Stepanov, A. Drezet, F. R. Aussenegg, A. Leitner, and J. R. Krenn, *Appl. Phys. Lett.* **88**, 094104 (2006).

<sup>10</sup>T. Holmgaard and S. I. Bozhevolnyi, *Phys. Rev. B* **75**, 245405 (2007).

<sup>11</sup>A. V. Krasavin and A. V. Zayats, *Appl. Phys. Lett.* **90**, 211101 (2007).

<sup>12</sup>B. Steinberger, A. Hohenau, H. Ditlbacher, F. R. Aussenegg, A. Leitner, and J. R. Krenn, *Appl. Phys. Lett.* **91**, 081111 (2007).

<sup>13</sup>A. V. Krasavin and A. V. Zayats, *Phys. Rev. B* **78**, 045425 (2008).

<sup>14</sup>T. Holmgaard, S. I. Bozhevolnyi, L. Markey, and A. Dereux, *Appl. Phys. Lett.* **92**, 011124 (2008).

<sup>15</sup>T. Holmgaard, Z. Chen, S. I. Bozhevolnyi, L. Markey, A. Dereux, A. V. Krasavin, and A. V. Zayats, *Opt. Express* **16**, 13585 (2008).

<sup>16</sup>T. Holmgaard, S. I. Bozhevolnyi, L. Markey, A. Dereux, A. V. Krasavin, P. Bolger, and A. V. Zayats, *Phys. Rev. B* **78**, 165431 (2008).

<sup>17</sup>A. Yariv, *Electron. Lett.* **36**, 321 (2000).

<sup>18</sup>S. I. Bozhevolnyi, V. S. Volkov, E. Devaux, J.-Y. Laluet, and T. W. Ebbesen, *Nature (London)* **440**, 508 (2006).

<sup>19</sup>S. Jetté-Charbonneau, R. Charbonneau, N. Lahoud, G. Mattiussi, and P. Berini, *Opt. Express* **13**, 4674 (2005).

<sup>20</sup>S. I. Bozhevolnyi, A. Boltasseva, T. Søndergaard, T. Nikolajsen, and K. Leosson, *Opt. Commun.* **250**, 328 (2005).